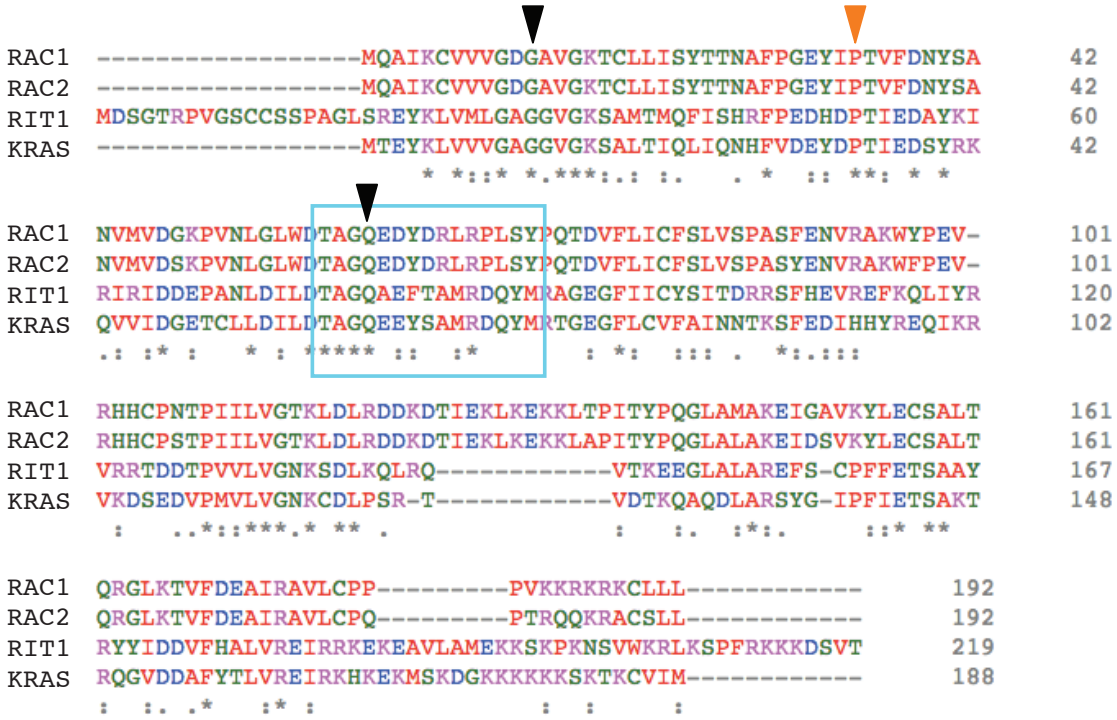

Supplementary Figure 1 | Protein sequence alignment of RAC, RAS, and RIT1 small GTPases. Protein sequence alignment of RAC1, RAC2, KRAS, and RIT1 sequences generated using ClustalW[54]. The numbers on the right indicate amino acid position. *, identical amino acid. **:**, strongly similar amino acid. ·, weakly similar amino acid. Black arrows indicate the G12 and Q61 mutation hotspots in *KRAS*. An orange arrow indicates the P29 hotspot in *RAC1*. A blue box indicates the switch II domain mutational hotspot identified in *RIT1* in the present study. Sequences were obtained from www.ensembl.org and correspond to the following transcripts: RAC1, ENST00000348035. RAC2, ENST00000249071. KRAS, ENST00000311936. RIT1, ENST00000368323.

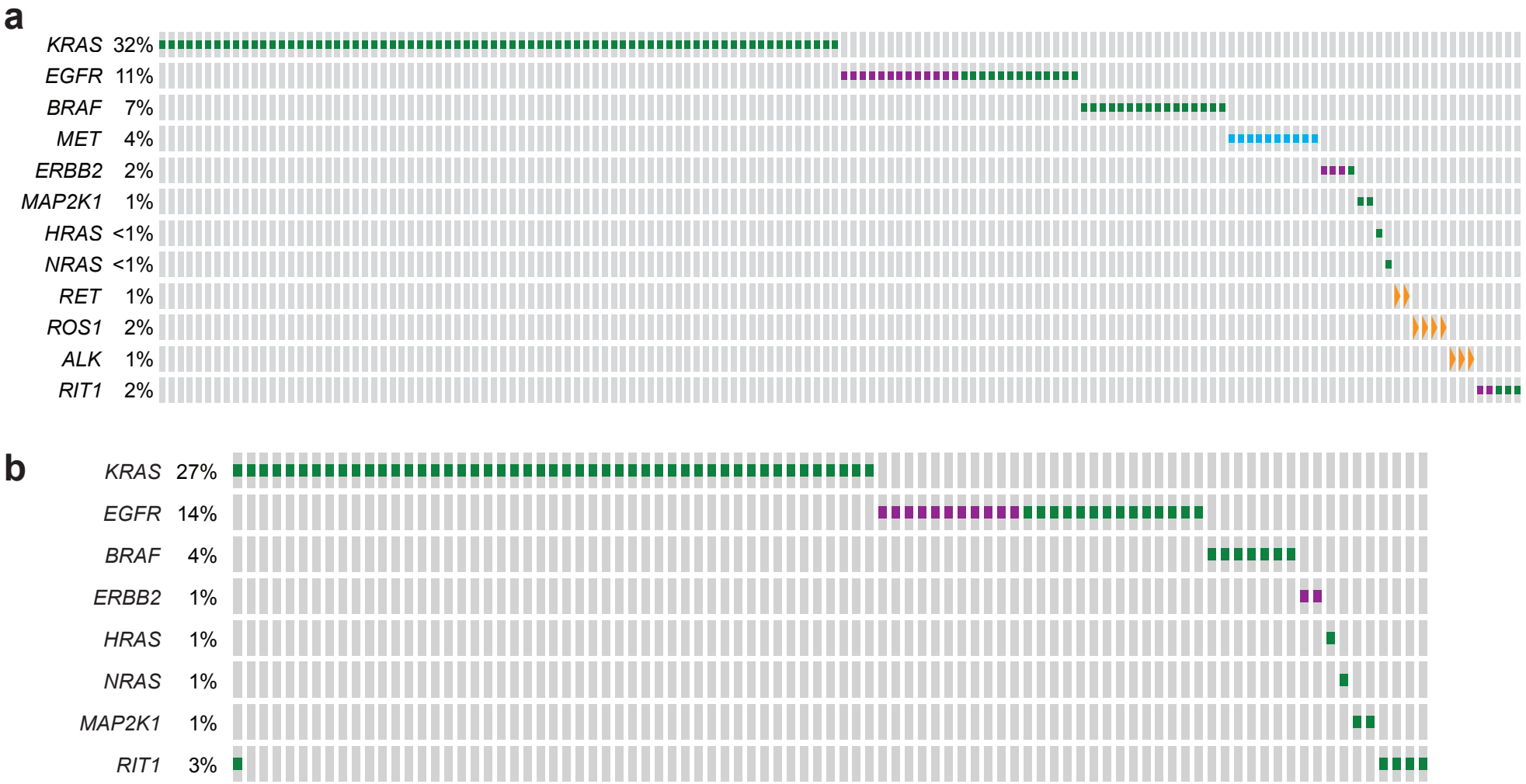

Supplementary Figure 2 | Mutual exclusivity of *RIT1* and other driver mutations in lung adenocarcinoma. **a,** Depiction of mutation data from 230 samples from The Cancer Genome Atlas lung adenocarcinoma sequencing study, displayed using the MSKCC cBio portal (http://cbio.mskcc.org). Each column represents a sample; each row corresponds to a different gene. Samples lacking alterations in the genes shown are not displayed. Green box: missense mutation present, purple box: in-frame insertion/deletion, orange triangles: fusion event, blue box: *MET* exon 14 skipping. For all genes except *RIT1*, only mutations of known significance are displayed. Numbers indicate the percentage of samples in the cohort with mutation in the respective gene. **b,** Data from 183 lung adenocarcinomas described in Imielinski et al.[1], depicted as in (**a**). Fusion genes and exon skipping were not analyzed.

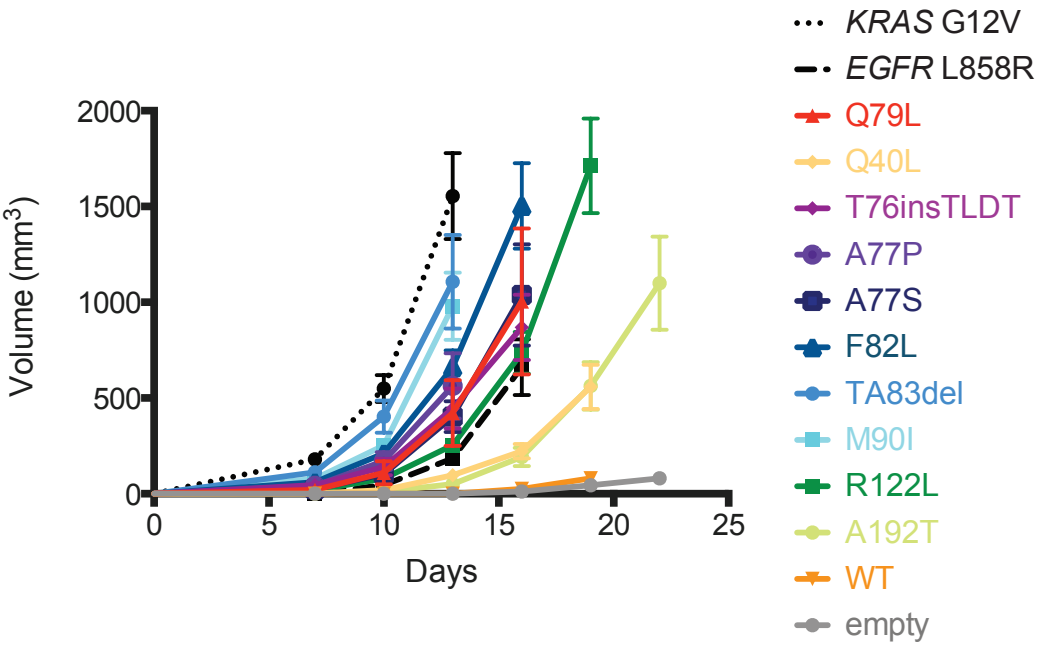

Supplementary Figure 3 | Transforming capability of somatic *RIT1* mutants. NIH3T3 cells were transduced with retrovirus to induce expression of wild-type *RIT1* (WT), mutated RIT1, empty vector, or known oncogenic mutations (*KRAS* G12V, *EGFR* L858R) as positive controls. After selection with puromycin, cells were expanded and $2x10^5$ cells injected per site subcutaneously into the flanks of nude mice. Beginning at day 7 post-injection, tumors were measured every three days with a digital caliper. Data shown is mean+SEM at each timepoint, n = 9 injection sites per condition.

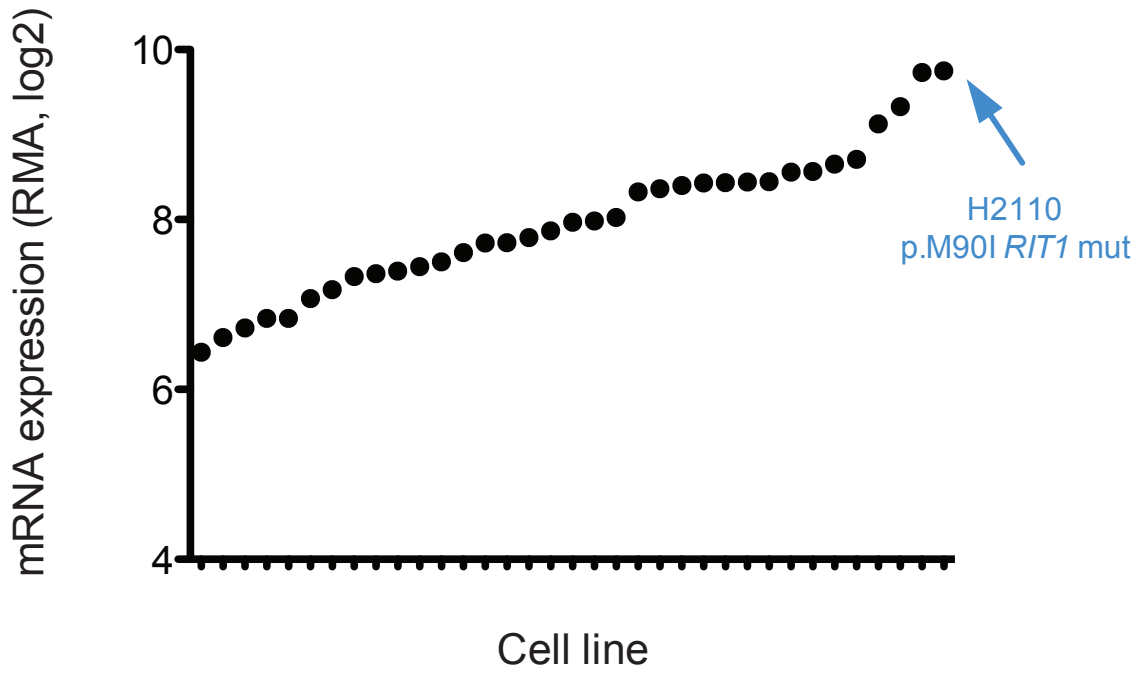

Supplementary Figure 4 | RNA expression of *RIT1* in driver-negative non-squamous NSCLC lines. We queried genotype data from the Cancer Cell Line Encyclopedia (CCLE) and identified 35 driver-negative non-squamous NSCLC lines with gene expression data (Supplementary Table 4). Data shown is the log2 robust multi-array average (RMA) of *RIT1*, generated as described[27] from the 35 cell lines, sorted in order of lowest to highest *RIT1* expression.

Berger et al. Supplementary Table 1

Dataset	Sample ID	Age	Gender	Histopathology Review	Stage	Protein change	mRNA change	Allelic fraction
Broad	LUAD-E00934	58	M	Acinar predominant Adc	IB	p.Q40L	c.119A>T	0.12
Broad	LUAD-S01345	74	M	Solid predominant Adc	IB	p.A77P	c.229G>C	0.13
Broad	LUAD-CHTN-MAD06-00490	36	F	Micropapillary predominant Adc	NA	p.M90I	c.270G>A	0.15
Broad	LUAD-S00499	72	F	Acinar predominant Adc	IIIA	p.R122L	c.365G>T	0.25
Broad	LUAD-NYU627	67	F	Papillary predominant Adc	IA	p.A192T	c.574G>A	0.17
TCGA	TCGA-44-6779	50	F	Solid predominant Adc	IIB	p.76_76T>TLDT	c.227_228insTTTGGATAC	0.16
TCGA	TCGA-55-1596	55	M	Solid predominant Adc	IIB	p.F82L	c.246T>G	0.38
TCGA	TCGA-73-4675	59	M	Micropapillary predominant Adc	IIIA	p.TA83del	c.248_253delCAGCCA	0.50
TCGA	TCGA-05-4384	66	M	Papillary predominant Adc	IIIA	p.M90I	c.270G>T	0.31
TCGA	TCGA-49-4514	79	F	Papillary predominant Adc	IA	p.M90I	c.270G>T	0.20

Supplementary Table 1. Clinical and genomic data of *RIT1*-mutated tumors identified in Broad[1] and TCGA datasets.

Berger et al. Supplementary Table 2

Tumor Type	n, samples	n, mutations	Reference
Glioblastoma	91	0	*44*
Prostate	103	0	*45*
Sarcoma	207	0	*46*
Ovarian	316	0	*47*
Breast	507	0	*48*
Squamous cell lung cancer	178	2	*49*
Colorectal	224	2	*50*
Pancreatic	142	0	*51*
Acute myelogenous leukemia	200	1 (p.M90I)	*52*
Endometrial	248	3	*53*
Cervical	36	1 (p.M90I)	*TCGA (unpublished)*

Supplementary Table 2. Survey of *RIT1* mutations in varied tumor types. Data from the eleven tumor types were queried in the MSKCC cbio portal (http://cbioportal.org) or from The Cancer Genome Atlas portal (tcga-portal.nci.nih.gov/) or from the references cited. Parentheses indicate specific amino acid changes also seen in the present study.

Berger et al. Supplementary Table 3

Variant	Tumor type	Reference	Soft agar	Foci
S10del	endometrial	COSMIC	-	-
K23E	salivary gland; lung adenocarcinoma	COSMIC; TCGA	+	n.d.
T38A	endometrial	COSMIC	+	+
R45Q	endometrial	COSMIC	-	-
D51V	chronic myelogenous leukemia	COSMIC	+	+
L74M	colon	COSMIC	+	+/-
E81G	myeloid malignancies	*23*	+	+
E81Q	melanoma; myeloid malignancies	COSMIC; *23*	+	+
F82C	myeloid malignancies	*23*	+	+
F82J	myeloid malignancies	*23*	+	+/-
F82V	myeloid malignancies	*23*	+	+/-
D87N	salivary gland	COSMIC	+	+
R112C	melanoma	COSMIC	-	-
P159F	melanoma	COSMIC	-	-
A165S	lung adenocarcinoma	TCGA	+/-	-
D173N	lung adenocarcinoma	TCGA	-	-

Supplementary Table 3. Transforming capability of *RIT1* mutations from diverse tumor subtypes. Somatic *RIT1* mutations were identified in the COSMIC database (v67)[26], reported in Gómez-Seguí et al.[23], or present in additional TCGA lung adenocarcinoma samples not analyzed in the 230 tumor study (https://tcga-data.nci.nih.gov/tcga/). NIH3T3 cells were transduced with retrovirus, selected with puromycin, and seeded in soft agar to determine colony-forming potential. Foci formation was determined after cells were grown to confluence in 10 cm dishes and transformed foci evaluated by quantification of foci in three fields/condition. +, significant colony or foci formation compared to wild-type RIT1 ($p < 0.05$ by one-tailed t-test). +/-, $p < 0.15$ by one-tailed t-test.

Berger et al. Supplementary Table 4 is included as an accompanying excel file.

Berger et al. Supplementary Table 5 is included as an accompanying excel file.

SUPPLEMENTARY REFERENCES

44. Comprehensive genomic characterization defines human glioblastoma genes and core pathways. *Nature* **455**, 1061-1068 (2008).
45. Taylor, B.S.*, et al.* Integrative genomic profiling of human prostate cancer. *Cancer Cell* **18**, 11-22 (2010).
46. Barretina, J.*, et al.* Subtype-specific genomic alterations define new targets for soft-tissue sarcoma therapy. *Nat Genet* **42**, 715-721 (2010).
47. Integrated genomic analyses of ovarian carcinoma. *Nature* **474**, 609-615 (2011).
48. Comprehensive molecular portraits of human breast tumours. *Nature* **490**, 61-70 (2012).
49. Hammerman, P.S.*, et al.* Comprehensive genomic characterization of squamous cell lung cancers. *Nature* **489**, 519-525 (2012).
50. Comprehensive molecular characterization of human colon and rectal cancer. *Nature* **487**, 330-337 (2012).
51. Biankin, A.V.*, et al.* Pancreatic cancer genomes reveal aberrations in axon guidance pathway genes. *Nature* **491**, 399-405 (2012).
52. Genomic and Epigenomic Landscapes of Adult De Novo Acute Myeloid Leukemia. *N Engl J Med* (2013).
53. Kandoth, C.*, et al.* Integrated genomic characterization of endometrial carcinoma. *Nature* **497**, 67-73 (2013).
54. Larkin MA, Blackshields G, Brown NP, Chenna R, McGettigan PA, McWilliam H *et al* (2007). Clustal W and Clustal X version 2.0. *Bioinformatics* **23:** 2947-2948.